Available online at www.sciencedirect.com
ScienceDirect
Journal of the European Ceramic Society 30 (2010) 1245–1251
www.elsevier.com/locate/jeurceramsoc

Characteristics of microbubbles generated by porous mullite ceramics prepared by an extrusion method using organic fibers as the pore former

Kiyoshi Okada [a,b,*], Mai Shimizu [a], Toshihiro Isobe [a], Yoshikazu Kameshima [a,1], Munetoshi Sakai [c], Akira Nakajima [a], Taisuke Kurata [d]

[a] *Department of Metallurgy and Ceramics Science, Tokyo Institute of Technology, 2-12-1 O-okayama, Meguro, Tokyo 152-8552, Japan*
[b] *Materials and Structures Laboratory, Tokyo Institute of Technology, 4459 Nagatsuta, Midori, Yokohama 226-8503, Japan*
[c] *Kanagawa Academy of Science and Technology, 308 East, Kanagawa Science Park, 3-2-1 Sakado, Takatsu, Kawasaki 213-0012, Japan*
[d] *Kurata Refractory Co. Ltd., Hirono, Futaba, Fukushima 979-0402, Japan*

Received 22 July 2009; received in revised form 16 October 2009; accepted 2 November 2009
Available online 2 December 2009

Abstract

Porous mullite ceramics with unidirectionally oriented pores were prepared by an extrusion method using rayon fibers as the pore formers and the characteristics of microbubbles generated by these porous ceramics were investigated. The 1200 mm long ceramics were tubular and of thick or thin types of 20–30 mm inner diameter and 30–50 mm outer diameter, respectively. The thin and thick samples had porosities of 47 and 49% and average pore radii of 7.8 μm. The gas permeabilities of the thick and thin samples were 4.1×10^{-14} and 5.4×10^{-14} m^2, respectively. Microbubbles were generated by introducing N_2 gas through the ceramic tube by immersing it into water. The minimum pressure (bubble point pressure) for generation of microbubbles was 20 kPa, much lower than for other bubble-forming methods. The average microbubble radii ranged from about 70 to 105 μm at flow rates of 0.15–0.25 L/min in the thin sample and 0.3–0.7 L/min in the thick sample. These bubble sizes are much smaller than calculated for a Fritz-type bubble such as generally formed by bubbling from pores and/or orifices. However, the present bubble sizes agree well with the calculated value based on nanobubbles, indicating that bubble formation occurs by mixing the gas with water in small pores. Since microbubbles enhance the dissolution rate of a gas phase in water, they are potentially useful for improving water environments, especially oxygen-deficient water. The effectiveness of gas dissolution in water was confirmed by determining the dissolution behavior of CO_2 gas using these porous ceramics.

Keywords: Extrusion; Porosity; Mullite; Functional applications; Microbubble

1. Introduction

Porous ceramics are generally prepared by a sintering method using pore formers[1] and/or by a partial sintering method.[2] It is however difficult to control the porous microstructures in materials prepared by these methods. We have previously reported a new and simple preparation method for controlling the pore orientation by an extrusion method using flammable fibers such as carbon fibers,[3] nylon fibers[4] or rayon fibers[5] as the pore formers. Since the fibers mixed in the paste become oriented during extrusion, unidirectionally aligned cylindrical pores are readily obtained after firing. Since the porous microstructure is controlled, the resulting porous ceramics have very high permeability and high mechanical strength.[6] These porous ceramics have been designated "lotus ceramics" because of the similarity of their porous microstructure to the root of the lotus plant.

One of the interesting properties of lotus ceramics is their excellent capillary action, derived from the unidirectional alignment and suitable size of the cylindrical pores.[7] The maximum capillary rise in these ceramics was about 1.3 m, nearly three times higher than previously reported for other porous materials.[5] The reasons for such excellent capillary behavior are thought to be the appropriate pore size, aligned through-hole porosity and cylindrical pore shape. This high capillary rise ability allows effective wetting of the surface of the lotus ceramics

* Corresponding author at: Materials and Structures Laboratory, Tokyo Institute of Technology, 4259, Nagatsuta, Midori, Yokohama 226-8503, Japan. Tel.: +81 45 924 5323; fax: +81 45 924 5338.
E-mail address: okada.k.ab@m.titech.ac.jp (K. Okada).
[1] Permanent address: Graduate School of Environmental Science, Okayama University, 1-1-1 Tsushimanaka, Okayama 700-8530, Japan.

0955-2219/$ – see front matter © 2009 Elsevier Ltd. All rights reserved.
doi:10.1016/j.jeurceramsoc.2009.11.003

without the need for electric pumping, and greatly suppresses the temperature increase in sunshine by the resulting water vapor evaporation, giving a temperature decrease of about 10 °C from a surface temperature of 40 °C.[8]

Since lotus ceramics have excellent gas permeability, they may also be good candidates as bubble generators. Bubbles are well known to improve oxygen-deficient water environments[9,10] and their effectiveness is enhanced with decreasing bubble size. Small bubbles have recently been called microbubbles (μm to sub mm in size) and nanobubbles (smaller than μm in size). Many bubble generation methods have therefore been investigated to obtain bubbles less than mm in size; these include the usage of fine nozzles, orifices and/or pores,[11–13] pressurizing dissolution methods,[14] multiphase flowing methods,[15,16] use of a special powerful shear rotating pump,[17] etc. In all cases, bubble generation requires highly pressurized gas (>400 kPa), powerful pumps and/or special pumps. The bubble size (Fritz bubble) generated by an orifice or pore using pressurized gas is represented by Eq. (1):

$$R_B = \left(\frac{3\gamma \cdot R_P}{2\rho \cdot g}\right)^{1/3} \quad (1)$$

where R_B is the bubble radius, γ is the surface tension, R_P is the orifice or pore radius, ρ is the density and g is the acceleration due to gravity. It is clear from Eq. (1) that microbubbles are difficult to generate by simply making the orifice or pore size smaller, because R_B is proportional to the 1/3 power of R_P, i.e. R_P must be 1000 times smaller to make R_B 1/10 times smaller. By contrast, Kukizaki and Goto[12] generated nanobubbles using various pore sizes in Shirasu porous glasses (SPG) and observed the following empirical relationship between pore and bubble radii:

$$R_B = 8.6R_P \quad (2)$$

Since the microstructure of SPG consists of uniform sized three-dimensionally connected mesopores, this unique microstructure is thought to be the main reason that nanobubbles can be generated with much smaller bubble size than calculated from Eq. (1).In this paper, the characteristics of bubbles generated using lotus ceramics were investigated under various conditions and the resulting bubble sizes were analyzed. The dissolution behavior of the bubbled gas was also investigated by using CO_2 gas and monitoring it with a CO_2 meter to simulate the effectiveness of bubbling for environmental water improvement.

2. Experimental procedures

2.1. Samples

The starting powders were alumina (Showa Denko, Japan), kaolin clay from Kentucky, USA (Morimura, Japan) and Chinese earthen clay (Inagaki Mining, Japan). The average particle sizes of these powders were 4.7, 1.0 and 20 μm, respectively. The Chinese clay was used to color the samples yellow-brown. The desired bulk chemical composition, achieved from appropriate mixtures of these three starting materials, was SO_2 = 36, Al_2O_3 = 56 and Fe_2O_3 = 5 mass%. The powder batch was dry mixed with 20 mass% rayon fibers (Hope RB3.3Dtex Tow, Omikenshi, Japan) of average fiber diameter 16.5 μm, chopped to 800 μm lengths by Chubu Pile Ind., Japan. The mixtures were kneaded with 40 mass% of water and molded using an extruder (Setogawa Industries, Japan) with a 95 mm barrel and inner aperture of 30 or 50 mm. Tubular green bodies with inner and outer diameters of 20–30 mm and 30–50 mm were extruded using an outlet die. The former and latter samples are designated thin and thick samples, respectively. The extruded green bodies were dried at room temperature for 3 days, then at 120 °C for 18 h before being fired at 1500 °C for 4 h in air.

The porosity of the samples was measured by the Archimedes technique using water. The pore size distribution and pore volume of the samples was measured by mercury intrusion porosimetry (Pascal 240, Carlo Elba, Italy) with a maximum injection pressure of about 200 MPa. For the calculation, the contact angle and surface tension of the Hg was taken as 130° and 0.485 N/m, respectively. The microstructure of the cut surface was observed using a scanning electron microscope (SEM; JSM-5310, JEOL Japan) and the crystalline phases in the samples were determined by powder X-ray diffraction (XRD; XRD-6100, Shimadzu, Japan) using monochromated Cu Kα radiation. The permeability of the samples was measured using home-built equipment and evaluated from Eq. (3):[5]

$$\Delta P = \frac{\eta \cdot L \cdot Q}{\mu \cdot A} \quad (3)$$

where ΔP is the pressure drop from entrance to exit of the sample, η is the dynamic viscosity of the liquid, L is the thickness of the sample, Q is the flow rate, μ is the Darcy's permeability and A is the cross-sectional area of the sample. The orientation angle (θ_P) of the cylindrical pores was calculated as reported elsewhere[4] using Eq. (4):

$$\cos\ \theta_P = \frac{d}{D} \quad (4)$$

where d is the diameter of the fiber and D is the maximum diameter of the elliptical pores observed by cross-sectional SEM micrographs. When the orientation of the pores is perfectly parallel to the extruded direction, the θ_P is 0°. The number of data points used for the measurement of θ_P was 300.

2.2. Bubble size measurements

A home-built bubbler was prepared using tubular lotus ceramics in a jig (Fig. 1). This bubbler was immersed in a water tank and dry N_2 gas was supplied from a cylinder (≤200 kPa) or air from a conventional air pump (MV-6005VP, Enomoto Micro Pump Co., Japan). The maximum pressure and flow rate of the air pump was 30.7 kPa and 4 L/min when used with a power supply delivering 100 V and 0.1 A. Both thick and thin lotus ceramics were used for the bubbler, at flow rates of 0.15, 0.20 and 0.25 L/min for the thin sample and 0.3, 0.5 and 0.7 L/min for the thick sample. The generated bubbles were recorded using a high-speed camera (1024-PC1 & 512PC1, Photron, Japan)

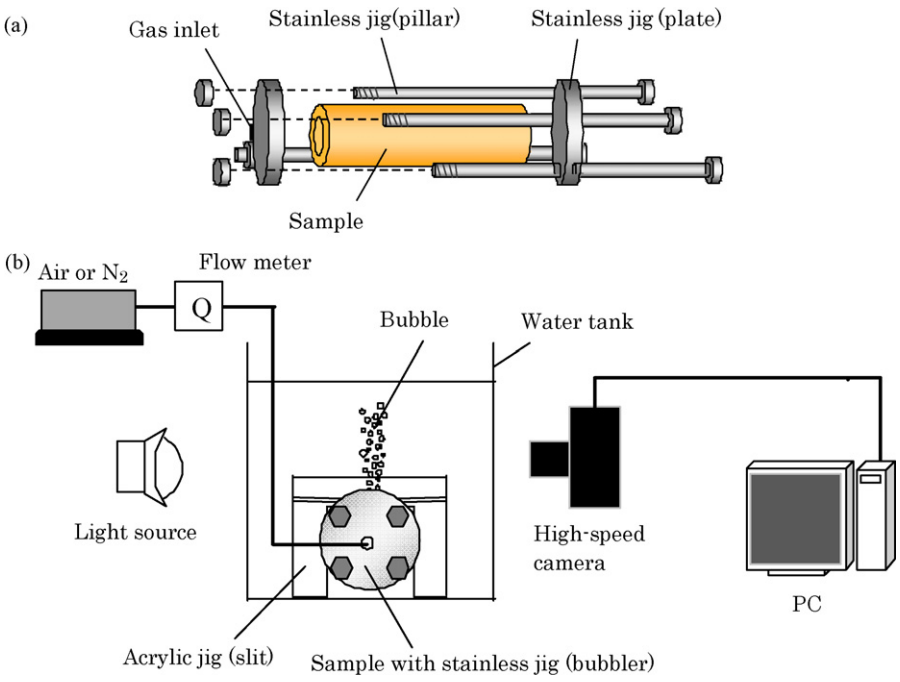

Fig. 1. Schematic illustration of experimental set up: (a) bubbler and (b) set up.

as shown in Fig. 1, with a recording rate and shutter speed of 1000 fps and 1/2000 s, respectively. The resulting photographs were analyzed using a DITECT system (DIPPMACRO-KAST, Japan). A slit was used to avoid overlap of the bubbles in this observation. The number of bubbles used for the bubble size distribution measurement varied according to the flow rate, and ranged from 176 to 562.

The bubble ascent velocity was determined for the thick sample from the moving distance of bubbles observed during a 15 ms time interval. The bubble ascent velocity was calculated from an average of 300–500 data points.

2.3. CO_2 bubbling

To examine effect of bubbling in water, CO_2 was bubbled in a water at a volume of 5 L and the CO_2 dissolution behavior was monitored using a CO_2 meter (CGP-1, TOA-DKK, Japan) and a pH meter (HM-21P, TOA-DKK, Japan). The bubbling experiments were performed using a thick sample, and reference measurements were also made using a commercial bubbler (GX-62, Gex Co., Japan) and a vinyl tube. The flow rate and pressure for bubbling were 0.5 L/min and 50 kPa, respectively.

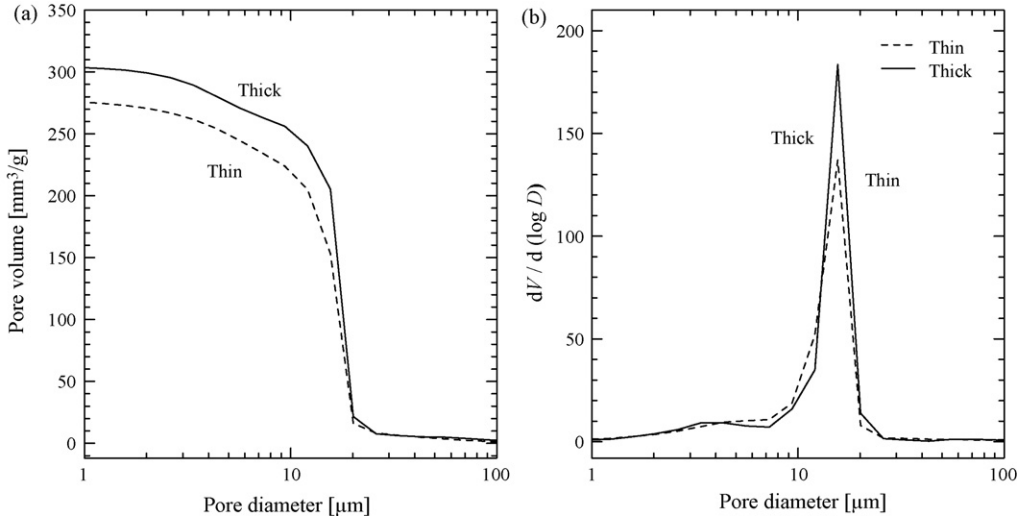

Fig. 2. Pore size distributions of the thin and thick samples.

Table 1
Porosity and gas permeability of samples.

Sample	Porosity (%)	Permeability ($\times 10^{-14}$ m^2)
Thin	47	4.1
Thick	49	5.4

3. Results and discussion

3.1. Characterization of the samples

The porosities of the samples (Table 1) were 47 and 49%, the slightly higher porosity pertaining to the thicker sample. The pore size distributions (PSDs) of the samples measured by Hg porosimetry are shown in Fig. 2. In this figure, PSD in Fig. 2(a) is calculated to show cumulative pore volume distribution while PSD in Fig. 2(b) is calculated to clearly show sharpness of the PSD. The total pore volume of the thick sample was higher than that of the thin sample and is in agreement with the porosities of the two samples. The both PSDs in Fig. 2(b) showed a sharp peak at 15–16 μm in pore diameter and these pores are thought to be those introduced by the fibers used as the pore former. The XRD pattern of the thin sample is shown in Fig. 3. The crystalline phase observed was mullite ($Al_{4+2x}Si_{2-2x}O_{10-x}$), only one stable phase in the Al_2O_3–SiO_2 system. The XRD pattern of the thick sample was very similar with that of the thin sample, thus, the crystalline phase of this sample was also mullite.

The SEM micrographs of the cross-sections of the thin and thick samples perpendicular and parallel to the extruded direction (Fig. 4) show many cylindrical pores formed by burnout of the rayon fibers. These cylindrical pores show considerable orientation parallel to the extrusion direction, but the average orientation angle (θ_P) of these samples is about 40°, with 80% of pores in the range θ_P = 10–50°. Thus, the cylindrical pores in these samples are not as well aligned along with the extrusion direction as in the case of the lotus ceramics previously reported ($\theta_P \approx 10°$).[3,4] This difference is attributed to the extruders used, the size of the extruded samples, the type of fiber and the particle sizes of the starting materials, etc. However, the present reasonable alignment of the pores may not be detrimental to the present application, for which the pores should be connected from the inside of the tube to the outside to generate bubbles; the declining orientation angle of the present cylindrical pores is also preferable for this application. This consideration was confirmed by the high permeability measured from the inside to the outside of the tubular samples (Table 1). These values of 4.1×10^{-14} and 5.6×10^{-14} m^2 are several hundred times higher than for conventional porous ceramics with similar porosity of 43%.[5]

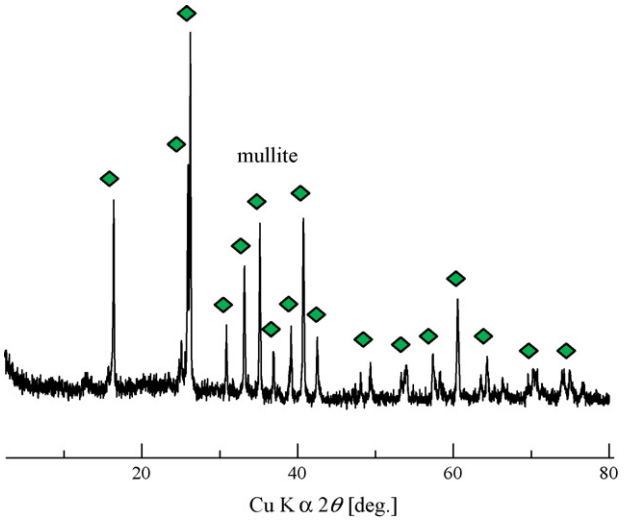

Fig. 3. XRD pattern of the thin sample.

Table 2
Bubble size and rising velocity of samples.

Sample	Flow rate (L/min)	Bubble radius (μm)	Data number	Rising velocity (mm/s)
	0.15	70	176	–
Thin	0.2	105	259	–
	0.25	110	522	–
	0.3	70	344	29
Thick	0.5	90	513	49
	0.7	95	560	46

3.2. Bubble size distribution

Generation of bubbles was observed by varying the gas pressure from 0 to 200 kPa, indicating a minimum pressure of 20 kPa. This minimum bubble generation pressure is lower than the pressure available from the conventional air pump used here, allowing it to be used to examine bubble generation. The bubble point pressure (P_B), corresponding to the minimum bubble generation pressure, can be calculated using Eq. (5):

$$P_B = \frac{2\sigma \cdot \cos\ \theta_C}{R_P} \quad (5)$$

The calculated P_B value of this sample is 6.4 kPa, setting R_P = 7.8 μm and θ_C = 70° as in Ref. [6], but this calculated value is much smaller than the observed value. The R_P calculated from the observed P_B is 2.5 μm and is much smaller than the observed R_P. The discrepancy between the observed and calculated P_B is uncertain in the present.

The bubble size distributions of the thin sample at flow rates of 0.15, 0.20 and 0.25 L/min are shown in Fig. 5(a) and those of the thick sample at flow rates of 0.30, 0.50 and 0.70 L/min are shown in Fig. 5(b). The average bubble sizes are listed in Table 2. In Fig. 5(a), the bubble size distribution becomes broader and the peak position becomes slightly larger with increasing flow rate. Thus, the average bubble radii (Table 2) increase from 70 to 105 and further to 110 μm with increasing flow rate. A similar trend is shown in Fig. 5(b) and the average bubble radii (Table 2) increase from 70, 90 and 95 μm with increasing flow rate. Bubble size, however, has no flow rate dependency based on the both Eqs. (1) and (2). Although we have no direct evidence for this reason, it is considered that the volume size of the gas phase mixing with water in the lotus ceramics may increase with higher the gas flow rate.

There are two reported relationships between pore size and bubble size, represented by Eqs. (1) and (2). These relation-

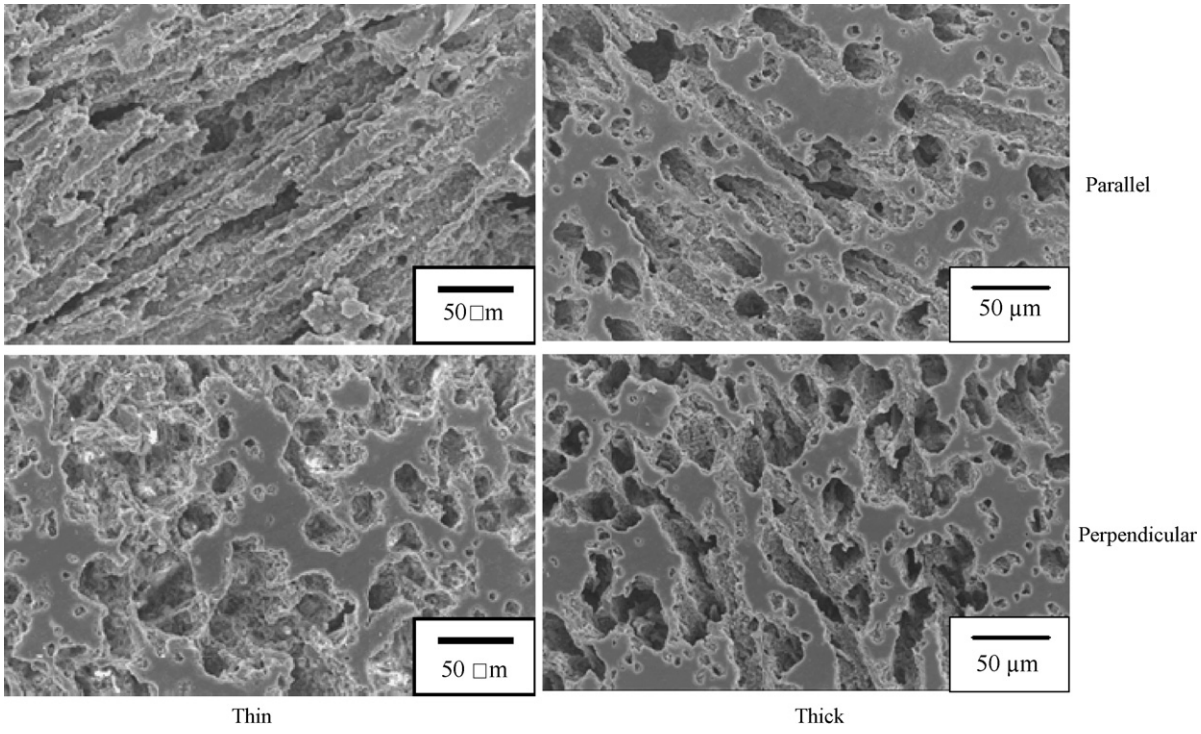

Fig. 4. Micrographs of the thin and thick samples perpendicular and parallel cross-sections to the extrusion direction.

ships are shown in Fig. 6. In the case of Fritz bubbles (Eq. (1)), the bubble size decreases only slightly with decreasing pore size. By contrast, large changes in bubble size proportional to changing pore size are predicted in the case of nanobubbles (Eq. (2)). Thus, the pore size effectively reflects the size of nanobubbles but not of Fritz bubbles. Here, the pore radii of the thin and thick samples were same 7.8 μm from the observed PSDs in Fig. 2(b) while the bubble radii were 70–110 μm as listed in Table 2. As plotted in Fig. 6, the results for the present samples are in better agreement with nanobubble behavior calculated from Eq. (2) than Fritz bubbles, calculated from Eq. (1). Kukizaki and Goto[12] have reported the generation of nanobubbles using Shirasu porous glass (SPG) with three-dimensionally connected pores (spinodal texture). On the basis of bubble generation through porous materials, the behavior of the present samples may be similar to that of SPG nanobubbles. When porous microstructures are immersed in water and gas is introduced into the water-filled pores, it mixes with the water in the pores and forms smaller bubbles than would be formed by two fluids in a nozzle or orifice, as in the generation of Fritz bubbles.

The average ascent velocities of gas bubbles in the thick sample at three different flow rates (Table 2) range from 29 to 49 mm/s and are in fair agreement with values calculated from

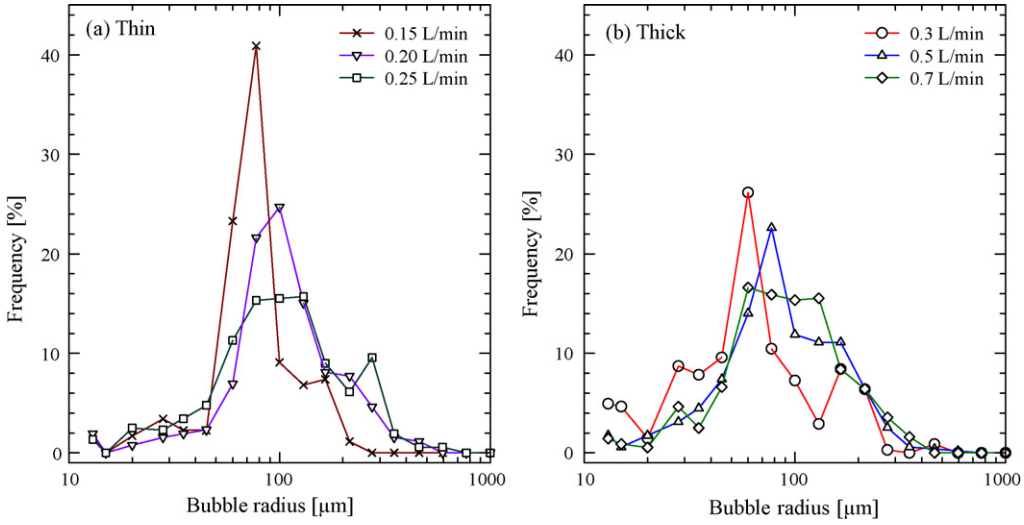

Fig. 5. Bubble size distributions of the thin (a) and thick samples (b) at three different flow rates.

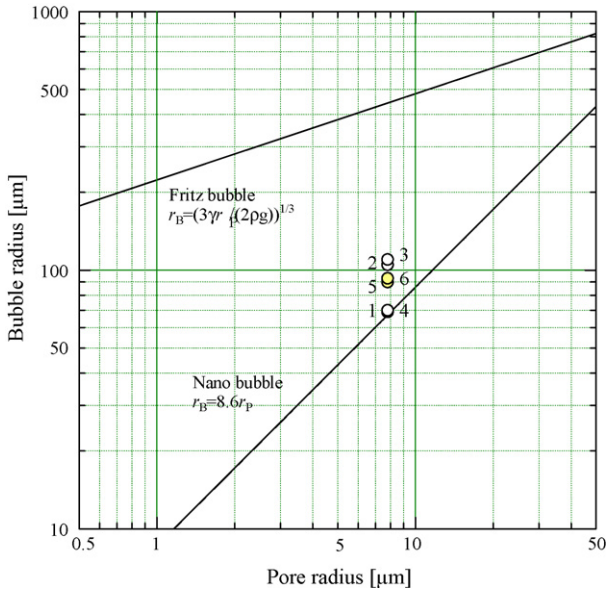

Fig. 6. Relationships between pore radius and bubble radius for Fritz bubbles (Eq. (1)) and nanobubbles (Eq. (2)). The numbers 1–3 for open circles represent thin samples with flow rates of 0.15, 0.20 and 0.25 L/min and those of 4–6 for colored circles represent thick samples with those of 0.3, 0.5 and 0.7 L/min, respectively.

Stokes' Law (Eq. (6)):

$$u = \frac{2(\rho_L - \rho_G)gR_B^2}{9\eta} \quad (6)$$

where u is the ascent velocity and ρ_L and ρ_G are the liquid and gas densities, respectively.

Compared with other bubbling equipments, the present bubbling method has the advantages of lower bubbling pressure, easier microbubble formation, use of a simpler system and ease of scaling up the bubbling area.

3.3. CO_2 bubbling

Changes of the CO_2 concentrations in water by the use of three different bubblers are shown in Fig. 7 as a function of bubbling time. All three bubblers showed increasing CO_2 concentrations in the water due to the partial dissolution of the bubbled CO_2. The concentration increases were linear with bubbling time in the initial stage for all three bubbling experiments, corresponding to a zero-order reaction, but the slopes of the lines were less steep in the experiments with the commercial bubbler and tube. This may be due to the higher concentration difference in the interface between the bubbles and the water because of the larger bubble sizes in the commercial bubbler and tube, delaying the dissolution by a diffusion effect.[18] Corresponding to the increase of CO_2 concentration in the water, the pH decreased from 6.0 to 4.0 in the lotus sample, 4.3 in the commercial bubbler and 4.4 in the tube. The linear rate constants of CO_2 concentration were different in the three bubbling experiments and increased in the order: tube (0.22 ppm/s) < commercial bubbler (0.32 ppm/s) < lotus ceramics (1.19 ppm/s). The rate constant for the lotus ceramics is

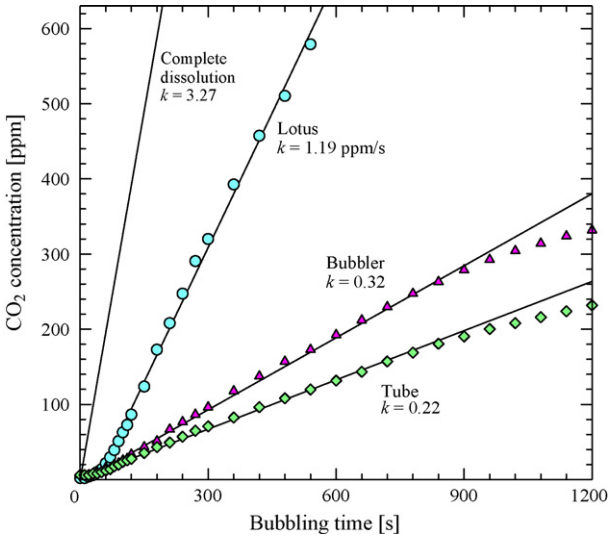

Fig. 7. Change of CO_2 concentration for the three different bubbling experiments.

thus much higher than for the other bubblers. Since the maximum rate constant at which all the bubbled CO_2 is dissolved in the water is 3.27 ppm/s, about 36% of the bubbled CO_2 is estimated to dissolve in the water (only about 50 cm in depth) by the lotus ceramics. The average bubble radius from the present lotus ceramics about 90 μm, while the bubble sizes formed by the reference bubblers were much larger, i.e. 1500 μm from the commercial bubbler and 3500 μm from the tube. Thus, the number of bubbles formed is much greater in the lotus ceramics and the surface area is higher than the other bubblers. The bubble ascent velocities calculated from the Stokes equation (Eq. (6)) for the bubbles from these three bubblers differ greatly, being 18, 4900 and 26,600 mm/s, respectively. In addition to the different bubble ascent velocities, the numbers of generated bubbles and the ratios of surface area to volume of these bubbles increase markedly with decreasing bubble size. These two factors are suggested to be the reason for the difference in the CO_2 concentration and pH of the water between the three bubblers.

The results of the present CO_2 bubbling experiments suggest that the lotus ceramics should be effective for applications such as suppressing the formation of bio-fouling,[9] removal of heavy metal ions as carbonates,[19] anesthesia agents for fish,[20] pH control for the safety of high pH water,[21] etc. Lotus ceramics are also considered to be effective for dissolving oxygen gas in oxygen-deficient water environments (under reducing conditions) and improving the BOD and COD of the water. The present bubbling system has the advantage of producing bubbles even with a weak power pump such as an air pump; it can therefore be used to oxygenate water environments with a pump powered by a conventional solar battery.

4. Conclusion

Lotus ceramics prepared by the extrusion method using fibers as the pore formers show high gas permeability, and the

characteristics of bubble generation using this lotus ceramics were investigated with the following results:

(1) The thin and thick lotus ceramics studied here had porosities of 47 and 49%, average pore radii of about 7.8 μm and gas permeabilities of 4.1×10^{-14} and 5.6×10^{-14} m^2, respectively.
(2) Bubbles could be generated at lower pressure (≥20 kPa) than with other bubbling methods, giving these materials an advantage.
(3) The resulting average bubble radii were 70–110 μm and the relationship between pore radius and bubble radius was in better agreement with that calculated for nanobubbles rather than Fritz bubble models.
(4) The average bubble acsent velocities were about 30–50 mm/s, in fair agreement with values calculated from Stokes' equation.
(5) The present lotus ceramics were effective in dissolving CO_2 in water because of their large surface area and slow bubble ascent velocity due to the small bubble size. They should therefore be effective in improving the quality of environmental waters by bubbling air through them.

Acknowledgements

The authors thank Professor K.J.D. MacKenzie of Victoria University of Wellington for critical reading and editing of this manuscript. We are also grateful to Professors M. Daimon and E. Sakai for permitting to use Hg porosimeter.

References

1. Wang HT, Liu XQ, Meng GY, Porous. α-Al_2O_3 ceramics prepared by gelcasting. *Mater Res Bull* 1997;**32**:1705–12.
2. Glass SJ, Green DJ. Permeability and infiltration of partially sintered ceramics. *J Am Ceram Soc* 1999;**82**:2745–52.
3. Isobe T, Tomita T, Kameshima Y, Nakajima A, Okada K. Preparation and properties of porous alumina ceramics with oriented cylindrical pores produced by an extrusion method. *J Eur Ceram Soc* 2006;**26**:957–60.
4. Isobe T, Kameshima Y, Nakajima A, Okada K, Hotta Y. Extrusion method using nylon 66 fibers for the preparation of porous alumina ceramics with oriented pores. *J Eur Ceram Soc* 2006;**26**:2213–7.
5. Okada K, Uchiyama S, Isobe T, Kameshima Y, Nakajima A, Kurata T. Capillary rise properties of porous mullite ceramics prepared by an extrusion method using organic fibers as the pore former. *J Eur Ceram Soc* 2009;**29**:2491–7.
6. Isobe T, Kameshima Y, Nakajima A, Okada K, Hotta Y. Gas permeability of the porous alumina ceramics with uni-directionally aligned pores by extrusion method. *J Eur Ceram Soc* 2007;**27**:53–9.
7. Kubota T, Sugimoto H, Komiya H. Research development of multiple functional greenized wall system using ceramic board with capillary rising property. *Report Obayashi Tech Inst* 2003;**67**:1–6.
8. Okada K, Kameshima Y, Nakajima A, Madhusoodana CD. Preparation of lotus-type porous ceramics with high water pump-up ability and its cooling effect by water vapor evaporation. *J Heat Island Inst Intern* 2007;**2**:1–5.
9. Nakamura H, Hamasaki A, Tsuji M, Goto E. Development of anti-biofoulding technology with no pollution by carbonic acid. *Tech Report Mitsubishi Heavy Ind* 2005;**37**:166–9.
10. Park J-Y, Choi Y-J, Moon S, Shin D-Y, Nam K. Microbubble suspension as a carrier of oxygen and acclimated bacteria for phenanthrene biodegradation. *J Hazard Mater* 2009;**163**:761–7.
11. Sadatomi M, Kawahara A, Kano K, Ohtomo A. Performance of a new micro-bubble generator with a spherical body in a flowing water tube. *Exp Therm Fluid Sci* 2005;**29**:615–23.
12. Kukizaki M, Goto M. Size control of microbubbles generated from Shirasu-porous glass (SPG) membranes. *J Membr Sci* 2006;**281**:386–96.
13. Shirota M, Imamura T, Kameda M. Formation of single bubbles from a submerged orifice using pulsed ultrasound wave. *Trans J Soc Mech Eng B* 2006;**72**:1220–7.
14. Yamada S, Yoshimi Y, Terada T, Ohno K, Minamikawa H. Study on oxygen supplying of the micro-bubbles generated by the pressurizing dissolution method. *Japan J Multiphase Flow* 2007;**21**:84–90.
15. Fujikawa S, Zhang R, Hayama S, Peng G. The control of micro-air-bubble generation by a rotational porous plate. *Int J Multiphase Flow* 2003;**29**:1221–36.
16. Shui L, Eijkel JCT, van den Berg A. Multiphase flow in microfluidic systems-control and applications of droplets and interfaces. *Adv Colloid Interf Sci* 2007;**133**:35–49.
17. Onari H. Fisheries experiments of cultivated shells using micro-bubbles techniques. *J Heat Transfer Soc Jpn* 2001;**40**:2–7.
18. Farajzadeh R, Zitha PLJ, Bruining J. Enhanced mass transfer of CO_2 into water: experiment and modeling. *Ind Eng Chem Res* 2009;**48**:6423–31.
19. Baba, Y., Japanese Patent JP2007-130591 (2007).
20. Yamamoto, T., Watanabe, K., Imai, S., Onuki, T., Iida, M., Hosokawa, T., Nakajima, A., Anesthesia effect of CO_2 gas for salmon using dryice and CO_2 cylinder. FRA Salmonid Res. Report, 2008, 2, 8–10.
21. Kureha Engineering Co., http://www.kureha-eng.co.jp/english/water.htm.